Effect of cantilever nonlinearity in nanoscale tensile testing

Weiqiang Ding,[a] Zaoyang Guo,[b),c)] and Rodney S. Ruoff[c),d)]
Department of Mechanical Engineering, Northwestern University, Evanston, Illinois, 60208

(Received 19 July 2006; accepted 8 December 2006; published online 14 February 2007)

Microcantilevers are widely used in micro-/nanoscale mechanics studies. The nonlinear response of a cantilever at large deflection is sometimes overlooked. A general study of cantilever beam nonlinearity under a variety of loading conditions was performed with analytical and finite element analyses. Analytical equations for the applied load and the cantilever deflection were obtained. The cantilever nonlinearity was found to increase with increasing cantilever deflection and/or angle of loading. Tensile tests were performed on templated carbon nanotubes (TCNTs) with a custom-made nanomanipulator inside a scanning electron microscope. Atomic force microscope (AFM) cantilevers were used to load the TCNTs and sense the force. During the tests the AFM cantilevers were loaded to relatively large deflections with nonvertical loads applied at the AFM tip. Based on the slope and the loading angle measurements, the breaking forces of the TCNTs were obtained through numerical integration of the analytical equations. A comparison was made between the load results obtained from linear and nonlinear analyses. The linear analysis was found to underestimate the applied load by up to 15%. © *2007 American Institute of Physics*. [DOI: 10.1063/1.2435064]

I. INTRODUCTION

Microsize cantilever beams are widely used in microelectromechanical systems (MEMS) and atomic force microscopy (AFM). They can serve as structural and force-sensing elements and as actuators. The AFM cantilever is commonly used as a force-sensing tool in studies of local surface forces, either directly with an AFM system[1,2] or with specialized testing platforms.[3–10] In our nanoscale tensile loading studies of one-dimensional (1D) nanostructures,[6–10] AFM cantilevers were used to measure the applied load. The load was calculated based on Hooke's law, i.e., by multiplying the force constant of the cantilever with its deflection at the free end.

Recently, we studied the tensile properties of templated carbon nanotubes (TCNTs).[11,12] Compared with other 1D nanostructures we have studied,[6,8–10] the TCNTs have relatively high breaking forces (>10 μN). With limited choices for cantilever force constants, the AFM cantilevers were of necessity loaded to relatively large deflections so as to break the TCNTs. In addition, there was misalignment of the specimen during the tests, so the applied loads were not perpendicular to the long axis of the cantilever. In this paper, we present our analysis of the nonlinear cantilever response as a combined result of large deflection and nonvertical loading in our tensile tests. Analytical expressions for the applied load and vertical deflections at the free end of the cantilever were derived. Based on the measured slope at the free end and "angle of misalignment" (loading angle), the true applied load and cantilever deflection were obtained through numerical integration of elliptic integrals.

In addition, a general study of cantilever beam nonlinearity under a variety of loading conditions was performed through analytical analysis and finite element analysis (FEA). The dependences of the relative estimation error in force from linear analysis on parameters such as loading angle and relative vertical deflection were investigated.

II. EXPERIMENTS

Nanoscale tensile loading of TCNT was done with a custom-made nanomanipulator[3] inside the vacuum chamber of a LEO 1525 scanning electron microscope (SEM). Two AFM chips were mounted on the two opposing positioning stages of the nanomanipulator [Fig. 1(a)]. An AFM chip with relatively soft cantilevers (Chip NSC 12, lengths of 350 and 300 μm and nominal force constants of 0.3 and 0.5 N/m, respectively; MikroMasch, Inc.) was mounted on the *X-Y* stage, and an AFM chip with more rigid cantilevers (Chip NSC 12, lengths of 90 and 110 μm and nominal force constants of 14.0 and 7.5 N/m, respectively; MikroMasch, Inc.) was mounted on the *Z* stage together with the TCNT source. Detailed descriptions of the experimental method have been presented elsewhere.[8,9]

Through nanomanipulation, a TCNT was picked up and also clamped between two opposing AFM tips [Fig. 1(b)] with a rapid electron beam induced deposition method.[13] It was then tensile loaded until fracture. As mentioned, the TCNTs required relatively large breaking force. A picomotor actuator (Model 8701, New Focus, Inc.) was used to actuate the AFM cantilever to induce large cantilever deflection. Note that we did not use the piezoelectric bimorph actuator for cantilever actuation as used previously[6,8–10] because of its shorter range of actuation.

[a)]Present address: Department of Mechanical and Aeronautical Engineering, Clarkson University, Potsdam, NY, 13699-5725; electronic mail: wding@clarkson.edu
[b)]Present address: Departments of Mechanical and Civil Engineering, University of Glasgow, Glasgow G12 8LT, Scotland; FAX: +44 (0) 141 330 4557; electronic mail: z.guo@eng.gla.ac.uk
[c)]Authors to whom correspondence should be addressed.
[d)]FAX: +1 847 491 3915; electronic mail: r-ruoff@northwestern.edu

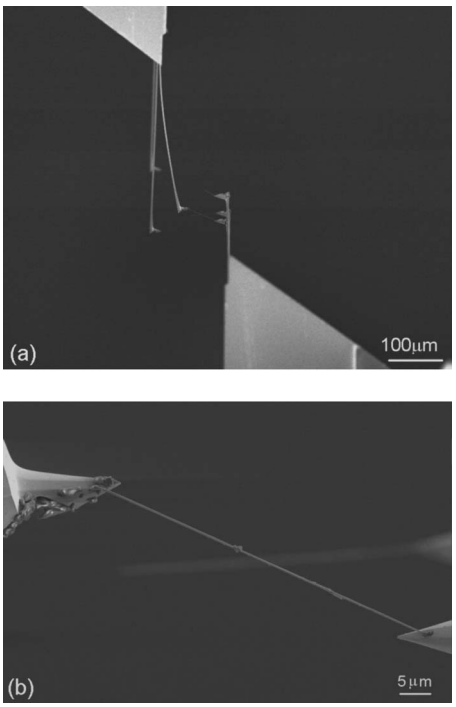

FIG. 1. (a) Low-magnification and (b) high-magnification SEM images of a TCNT being tensile loaded between two opposing AFM tips.

In our current experimental approach the tensile load and strain are not obtained during the loading process. During the test, the tensile load is increased in discrete steps, SEM images at each loading step are acquired, and the tensile load and strain are obtained from image analysis after the experiment is finished.

III. CANTILEVER DEFLECTION ANALYSIS

Compared with our previous work,[6,8–10] it is more difficult to determine the applied load from recorded SEM images for tensile tests on these TCNTs. Previously, the cantilever deflections were relatively small so that Hooke's law could be used to calculate the tensile load, and two methods were available to obtain the cantilever deflection through image analysis, one based on the calibration of the piezoelectric bimorph response and the other on the measurement of the slope at the free end. However, these methods cannot be used for the analysis of the tensile testing of the TCNTs presented here. The bimorph calibration method is not applicable because the force-sensing cantilevers were not actuated by the piezoelectric bimorph. The slope measurement method is also not applicable due to the cantilever nonlinearity.

At small deflection, we can obtain the vertical cantilever deflection (δ_y) and applied load (F) from the slope at the free end of the cantilever (ϕ_0) through linear analysis as

$$\delta_y = \tfrac{2}{3}\phi_0 L, \quad F = K\delta_y = \tfrac{2}{3}K\phi_0 L, \tag{1}$$

where $K=3EI/L^3$ is the force constant of the cantilever (E is the elastic modulus of the beam material, and I is the moment of inertia of the beam cross section). When the cantilever deflection is large, these relationships do not hold.

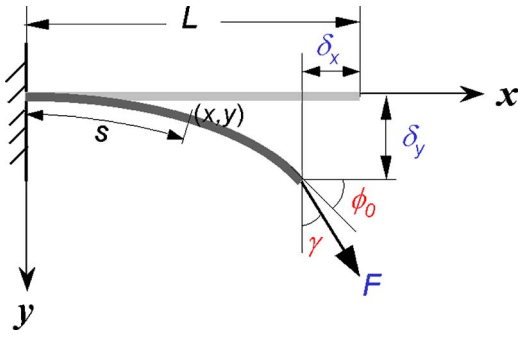

FIG. 2. (Color online) Large deflection of a cantilever beam with a nonvertical load applied at the free end.

The large deflection regime of a cantilever beam has been studied for several decades.[14–16] As demonstrated by Bisshopp *et al.*,[14] for a cantilever vertically loaded at the end to large deflection the applied load (F) and vertical deflection (δ_y) can also be represented by the slope at the free end (ϕ_0), but in a more complicated way than the linear case.

However, the result of Bisshopp *et al.*[14] cannot be directly applied to our experiments because the AFM cantilevers in our nanoscale tensile tests were not vertically loaded. As can be seen in Fig. 1, the TCNT was not perfectly aligned between the two opposing AFM tips. Sometimes the specimen was misaligned while being clamped to the AFM tips. The deflection of the cantilever also induces specimen misalignment. As can be seen in Fig. 2, with the deflection of the cantilever there is a displacement of the cantilever tip along the x direction (δ_x), which changes the orientation of the specimen attached to the cantilever.

Following the method of Bisshopp *et al.*,[14] we derived analytical expressions for the applied load and cantilever deflection for the cases of a nonvertically loaded cantilever.

Based on simple beam theory, the relationship between the bending curvature ($d\phi/ds$) and bending moment (M) of a uniform-section rectangular beam of linear elastic material at any point on the beam is given by

$$EI\frac{d\phi}{ds} = M. \tag{2}$$

As shown in Fig. 2, at a point on the beam with coordinates (x,y), the bending moment at the cross section is

$$M = F_y(L-\delta_x-x) - F_x(\delta_y - y), \tag{3}$$

where $F_x = F\sin\gamma$ and $F_y = F\cos\gamma$.

From Eqs. (2) and (3),

$$EI\frac{d\phi}{ds} = F_y(L-\delta_x-x) - F_x(\delta_y - y). \tag{4}$$

Differentiating Eq. (4) once with respect to s and dividing by EI on both sides,

$$\frac{d^2\phi}{ds^2} = -\frac{F_y}{EI}\frac{dx}{ds} + \frac{F_x}{EI}\frac{dy}{ds} = -\frac{F_y}{EI}\cos\phi + \frac{F_x}{EI}\sin\phi. \tag{5}$$

Multiplying both sides by $d\phi/ds$,

$$\frac{d^2\phi}{ds^2}\frac{d\phi}{ds} = \left(-\frac{F_y}{EI}\cos\phi + \frac{F_x}{EI}\sin\phi\right)\frac{d\phi}{ds}. \tag{6}$$

Rearranging Eq. (6),

$$\frac{d}{ds}\left[\frac{1}{2}\left(\frac{d\phi}{ds}\right)^2 + \frac{F_y}{EI}\sin\phi + \frac{F_x}{EI}\cos\phi\right] = 0. \tag{7}$$

Thus,

$$\frac{1}{2}\left(\frac{d\phi}{ds}\right)^2 + \frac{F_y}{EI}\sin\phi + \frac{F_x}{EI}\cos\phi = C. \tag{8}$$

Rearranging Eq. (8) and using the following relationship, $F_x = F\sin\gamma$ and $F_y = F\cos\gamma$, yields

$$\frac{1}{2}\left(\frac{d\phi}{ds}\right)^2 + \frac{F}{EI}\sin(\phi+\gamma) = C. \tag{9}$$

Using the boundary condition $M(L)=0$, from Eq. (2) one obtains $d\phi/ds|_{s=L}=0$. Therefore, from Eq. (9),

$$C = \frac{F}{EI}\sin(\phi_0+\gamma). \tag{10}$$

Inserting Eq. (10) into Eq. (9) yields

$$\frac{1}{2}\left(\frac{d\phi}{ds}\right)^2 = \frac{F}{EI}[\sin(\phi_0+\gamma) - \sin(\phi+\gamma)], \tag{11}$$

where $0 \leqslant \phi \leqslant \phi_0$. Equation (11) requires that $\phi_0+\gamma \leqslant \pi/2$, which means that the loading angle γ cannot be larger than $\pi/2-\phi_0$. This restriction is straightforward, as shown in Fig. 2.

Given that $\sin(\phi_0+\gamma) \geqslant \sin(\phi+\gamma)$, Eq. (11) can be converted to

$$\frac{d\phi}{ds} = \sqrt{\frac{2F}{EI}[\sin(\phi_0+\gamma) - \sin(\phi+\gamma)]}. \tag{12}$$

Rearranging Eq. (12) and integrating both sides (assuming the length of the beam remains constant) yields

$$\int_0^{\phi_0}\frac{1}{\sqrt{\sin(\phi_0+\gamma)-\sin(\phi+\gamma)}}d\phi = \sqrt{\frac{2F}{EI}}\int_0^L ds = \sqrt{\frac{2FL^2}{EI}}. \tag{13}$$

From Eq. (13) the representation of the load applied at the free end is

$$F = \frac{EI}{2L^2}\left[\int_0^{\phi_0}\frac{1}{\sqrt{\sin(\phi_0+\gamma)-\sin(\phi+\gamma)}}d\phi\right]^2. \tag{14}$$

The analytical representation of vertical deflection at the free end of the cantilever (δ_y) can be obtained as follows:

$$\frac{dy}{ds} = \frac{dy}{d\phi}\frac{d\phi}{ds} = \sin\phi. \tag{15}$$

Using Eq. (12),

$$\frac{dy}{d\phi}\sqrt{\frac{2F}{EI}}\sqrt{\sin(\phi_0+\gamma)-\sin(\phi+\gamma)} = \sin\phi. \tag{16}$$

From Eq. (16) the analytical expression for the vertical deflection at the free end can be derived as

$$\delta_y = \int_0^y dy = \sqrt{\frac{EI}{2F}}\int_0^{\phi_0}\frac{\sin\phi}{\sqrt{\sin(\phi_0+\gamma)-\sin(\phi+\gamma)}}d\phi. \tag{17}$$

Equations (14) and (17) are elliptic integrals that can be evaluated numerically, as demonstrated by Bisshopp *et al.*[14] Defining

$$\phi' = \phi+\gamma, \quad \phi_0{}' = \phi_0+\gamma,$$
$$1+\sin\phi' = 2k^2\sin^2\theta = (1+\sin\phi_0{}')\sin^2\theta, \tag{18}$$

it is possible to show

$$\begin{aligned}
&\int_0^{\phi_0}\frac{1}{\sqrt{\sin(\phi_0+\gamma)-\sin(\phi+\gamma)}}d\phi \\
&= \int_\gamma^{\phi_0{}'}\frac{1}{\sqrt{\sin\phi_0{}'-\sin\phi'}}d\phi' \\
&= \int_{\theta_1}^{\pi/2}\frac{1}{\sqrt{(2k^2-1)-(2k^2\sin^2\theta-1)}} \\
&\quad\times d[\arcsin(2k^2\sin^2\theta-1)] \\
&= \sqrt{2}\int_{\theta_1}^{\pi/2}\frac{1}{\sqrt{1-k^2\sin^2\theta}}d\theta,
\end{aligned} \tag{19}$$

where

$$k = \sqrt{[1+\sin(\phi_0+\gamma)]/2}$$

and

$$\theta_1 = \arcsin(\sqrt{(1+\sin\gamma)/[1+\sin(\phi_0+\gamma)]})$$

are two parameters for elliptic integrals. The integral expression in Eq. (19) can be converted into elliptic integrals as follows:

$$\begin{aligned}
&\int_{\theta_1}^{\pi/2}\frac{1}{\sqrt{1-k^2\sin^2\theta}}d\theta \\
&= \int_0^{\pi/2}\frac{1}{\sqrt{1-k^2\sin^2\theta}}d\theta - \int_0^{\theta_1}\frac{1}{\sqrt{1-k^2\sin^2\theta}}d\theta \\
&= F(k) - F(\theta_1,k),
\end{aligned} \tag{20}$$

where $F(k)$ and $F(\theta,k)$ are complete and incomplete elliptic integrals of the first kind. From Eqs. (14), (19), and (20), the elliptical integral representation of the load can be obtained as

$$F = \frac{EI}{L^2}[F(k) - F(\theta_1,k)]^2. \tag{21}$$

The integral expression in Eq. (17) for the vertical deflection at the free end can also be converted into elliptic integrals following the same process:

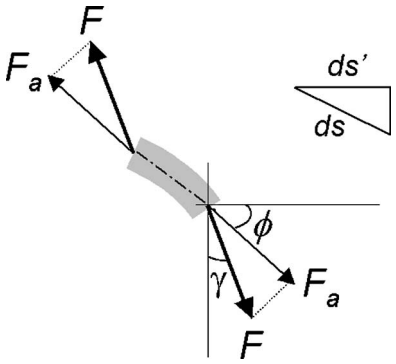

FIG. 3. The extension of a beam section under tension.

$$\int_0^{\phi_0} \frac{\sin\phi}{\sqrt{\sin(\phi_0+\gamma)-\sin(\phi+\gamma)}}d\phi$$
$$= \int_\gamma^{\phi_0'} \frac{\sin(\phi'-\gamma)}{\sqrt{\sin\phi_0'-\sin\phi'}}d\phi'$$
$$= \sqrt{2}\int_{\theta_1}^{\pi/2}\left(\frac{2k^2\sin^2\theta-1}{\sqrt{1-k^2\sin^2\theta}}\cos\gamma-2k\sin\theta\sin\gamma\right)d\theta$$
$$= \sqrt{2}[-2E(k)+2E(\theta_1,k)+F(k)-F(\theta_1,k)]$$
$$\times\cos\gamma-2\sqrt{2}k\cos\theta_1\sin\gamma, \tag{22}$$

where $E(k)$ and $E(\theta,k)$ are complete and incomplete elliptic integrals of the second kind. Inserting Eqs. (21) and (22) into Eq. (17), the elliptic integral representation of the vertical deflection at the free end is obtained as

$$\delta_y = \left\{\left[1-2\frac{E(k)-E(\theta_1,k)}{F(k)-F(\theta_1,k)}\right]\times\cos\gamma-\frac{2k\cos\theta_1}{F(k)-F(\theta_1,k)}\sin\gamma\right\}L. \tag{23}$$

The analytical representation for the horizontal deflection at the free end (δ_x) can be derived in the same manner. Starting from the following relationship:

$$\frac{dx}{ds}=\frac{dx}{d\phi}\frac{d\phi}{ds}=\cos\phi, \tag{24}$$

the elliptical integral representation for horizontal deflection is obtained as

$$\delta_x = L-\int_0^x dx = L-\sqrt{\frac{EI}{2F}}\int_0^{\phi_0}\frac{\cos\phi}{\sqrt{\sin(\phi_0+\gamma)-\sin(\phi+\gamma)}}d\phi$$
$$= \left\{1-\left[1-2\frac{E(k)-E(\theta_1,k)}{F(k)-F(\theta_1,k)}\right]\sin\gamma-\frac{2k\cos\theta_1}{F(k)-F(\theta_1,k)}\cos\gamma\right\}L. \tag{25}$$

In the above analysis it was assumed that the cantilever length remains constant. The actual length of the cantilever at deflection, however, can be obtained as follows. The tensile load component along the longitudinal axis of the cantilever beam induces an elongation of the beam. As shown in Fig. 3, for a short beam section, the force component along its longitudinal axis is given by

$$F_a = F\sin(\phi+\gamma). \tag{26}$$

The corresponding strain in this section is given by

$$\varepsilon_a = \frac{\sigma_a}{E}=\frac{F_a}{EA}, \tag{27}$$

where A is the cross-sectional area of the beam. Therefore,

$$\frac{ds}{ds'}=1+\varepsilon_a=1+\frac{F_a}{EA}. \tag{28}$$

The actual length of the beam under tension can be obtained through integration as

$$\int_0^L ds=\int_0^L\left(1+\frac{F_a}{EA}\right)ds'=L+\frac{F}{EA}\int_0^L\sin(\phi+\gamma)ds'. \tag{29}$$

Since $\sin(\phi+\gamma)<\sin(\phi_0+\gamma)<1$, the upper bound of the actual beam length is $(1+F/EA)L$, which is the case where the load is applied along the long axis of the cantilever beam.

IV. EXPERIMENTAL RESULTS

From the recorded high-resolution SEM images, the slope at the free end of the cantilever (ϕ_0) and the angle of loading (γ) were measured with high accuracy. From these two parameters the parameters k and θ_1 for the elliptical integrals were calculated. The load applied at the free end (F) and the corresponding cantilever deflections at the free end (δ_y, δ_x) were then obtained with Eqs. (21), (23), and (25), respectively. The elliptical integrals in these expressions were numerically integrated with a MATLAB program.[17]

As mentioned previously, the tensile load was increased in discrete steps and SEM images were taken at each loading step. The slope and loading angle at the last loading step were used to calculate the breaking force of the TCNT and the maximum cantilever deflection. The maximum vertical cantilever deflection was also obtained through image analysis by comparing the position of the end of the cantilever at the last loading step and its position after fracture. The cantilever deflection calculated through analytical analysis agrees reasonably well with the deflection measured from SEM images.

For samples 1, 2, and 4, the TCNTs fractured right after the last step of increase of load before any SEM image could be acquired. In these cases, the slope and loading angle from the step just before the last step were used to calculate the load and deflection through analytical analysis. The load and deflections obtained are then lower than the true values. Similarly, the cantilever position at the step just before the last step was used in image analysis to get the cantilever deflection. Such a practice can under- or overestimate the cantilever deflection because the end of the cantilever may slightly move forward or backward at each loading step, depending on the specific loading condition.

Another issue that needs to be considered in the analysis of the AFM cantilever loading is the loading position. In the analytical analysis the load is applied at the free end of a

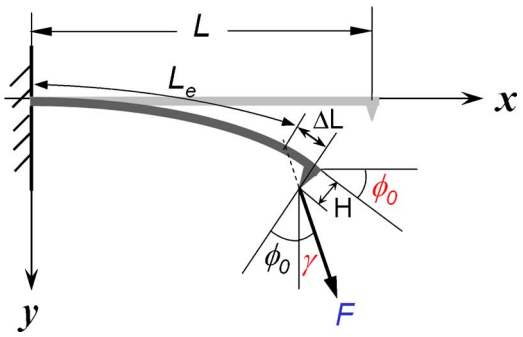

FIG. 4. (Color online) Large deflection of an AFM cantilever with a nonvertical load applied at the AFM tip.

cantilever beam (Fig. 2), but in the experiments the load was applied at the AFM tip (Fig. 1). Compared with the end-load case, applying the load at the AFM tip induces an additional bending moment for the nonvertical loading condition. This issue has been presented elsewhere,[8] but the beam nonlinearity was not considered.

Considering the beam deformation, the bending moment at a point (x,y) on the beam is

$$M = F_y(L - \delta_x - H\sin\phi_0 - x) - F_x(\delta_y + H\cos\phi_0 - y), \tag{30}$$

where H is the height of the AFM tip. The same analysis procedure [Eqs. (4)–(9)] can be applied but the boundary condition becomes $M(L) = -FH\sin(\phi_0 + \gamma)$. Because of the complicated boundary condition, it is not possible to obtain a simple analytical representation for the load F. Comparing the two bending moment expressions [Eqs. (3) and (30)], we can see that under the same loading condition, applying the load at the AFM cantilever tip results in a smaller bending moment than applying the load at the end of the cantilever. Therefore, using the end-loaded cantilever configuration to analyze our experiments will underestimate the applied load. Here, we propose a simple way to approximate the result by assuming that the load is applied at the free end of a cantilever beam of length L_e, as shown in Fig. 4. The *effective beam length* L_e is given by $L_e = L - \Delta L = L - H\tan(\phi_0 + \gamma)$. For positive angle of loading, this effective cantilever beam is shorter and stiffer than the actual AFM cantilever beam. The approximated load is thus higher than the one obtained with the end-loaded configuration that does not consider the AFM tip. Further analysis is needed in order to get the exact applied load values.

Table I compares the results from nonlinear analysis with those obtained from linear analyses. The additional bending moment introduced due to the presence of the AFM tip is considered in both linear and nonlinear analyses, and the effective beam length is used for numerical integration in nonlinear analysis. As shown, the linear analysis underestimates the applied load by up to 15%. The specimen misalignment (loading angle) induces significant nonlinearity. For example, samples 1 and 4 have similar deflection, but sample 1 was loaded with a larger loading angle. As a result, there is much larger error for sample 1 than for sample 4 by assuming linear force estimation.

With the knowledge of the applied load, the cantilever length change during the tensile testing can be estimated. The applied load is on the order of tens of micronewtons (Table I), and the cross-sectional area of the cantilever beam is 7×10^{-11} m^2 (35 μm wide, 2 μm thick). The elastic modulus of the silicon cantilever for the [110] direction (according to the commercial supplier, MikroMasch, Inc.) is around 169 GPa.[18] The upper bound of the strain in the cantilever is $\approx10^{-5}$. Therefore, the invariant beam length assumption is valid.

The inner and outer diameters of the TCNTs were measured in the SEM, and their fracture strengths were calculated and are listed in Table II. Without the SEM images of the last loading steps, the fracture strengths of samples 1, 2, and 4 are underestimated. Another issue that affects the measurement of strength is the stress concentration at the clamps. The reader is referred to Refs. 9 and 19 for detailed discussions of stress concentration effects. Overall, the measured fracture strengths of these amorphous carbon nanotubes are within the same range as those of amorphous carbon nanofibers we have previously studied.[7]

V. DISCUSSION

Micro-/nanocantilever beams are commonly encountered in nanoscale mechanics studies, either as the testing tool (e.g., an AFM cantilever) or as the sample itself (e.g., canti-

TABLE I. Tensile testing results on TCNTs from linear and nonlinear analyses.

Sample No.	Slope ϕ_0	Loading angle γ	Applied load F			Vertical deflection δ_y		
	(deg)	(deg)	Linear (μN)	Nonlinear (μN)	Error (%)	Measured[a] (μm)	Linear (μm)	Nonlinear[b] (μm)
1[c]	12.1	36.8	26.7	31.3	14.6	42.9	42.2	40.9
2[c]	17.4	5.5	24.6	25.4	3.0	68.7	70.8	69.5
3	9.2	42.0	22.0	25.4	13.3	30.6	32.2	31.3
4[c]	11.6	2.0	20.5	20.2	1.7	41.4	40.5	40.1
5	15.0	24.3	29.2	32.7	10.9	52.9	52.4	51.1

[a]The length of cantilever used to load TCNT 2 was 350 μm; for TCNTs 1 and 3–5, the length was 300 μm.
[b]Obtained by adding the deflection at the end of the effective cantilever beam with the deflection of the free extending portion $[H\tan(\phi_0+\gamma)\sin\phi_0]$.
[c]The last loading step was not captured.

TABLE II. Fracture strengths of TCNTs from linear and nonlinear analyses.

		Linear analysis		Nonlinear analysis	
Sample No.	Diameter (nm)	Load (μN)	Strength (MPa)	Load (μN)	Strength (MPa)
1[a]	350	26.7	400	31.3	460
2[a]	216	24.6	720	25.4	740
3	360	22.0	310	25.4	360
4[a]	358	20.5	290	20.2	290
5	280	29.2	580	32.7	650

[a]The last loading step was not captured.

levered nanostructures). Microcantilever beams are widely used as force-sensing elements in micro-/nanoscale testing devices,[4–10,20] and the loads are typically calculated based on Hooke's law. Cantilevered nanostructures have been tested with bending tests to evaluate their elastic moduli according to the simple beam theory.[21,22] In each of these cases, the nonlinear response of the cantilever beam/cantilevered nanostructure due to large deflection and/or nonvertical loading is sometimes overlooked. Here, we investigated the nonlinear response of a cantilever beam under different loading conditions through a detailed comparison of the load and deflection values from linear versus nonlinear analysis. The external load is assumed to be applied at the free end of the cantilever beam.

Besides nonlinear analytical analysis, FEA was used to study the nonlinear response of a cantilevered beam to a concentrated nonvertical load applied at the free end. A microcantilever beam model was built with ABAQUS (ABAQUS, Inc.) with dimensions of 300 μm length, 35 μm width, and 2 μm thickness. The elastic modulus of the silicon cantilever is assumed to be 169 GPa (Ref. 18) (the [110] direction, according to the commercial supplier, MikroMasch, Inc.). The same parameters were used in the MATLAB numerical integration program as in the analytical analysis discussed above. As will be shown in the next section, the load and deflection results from both FEA and analytical analysis were normalized to yield nondimensional parameters so that the results can be applied to any beam (thus for a variety of dimensions and physical properties, but with the beam made of linear elastic material). With the FEA model the response of this modeled cantilever beam loaded at the free end was obtained with the loading angles of –45°, 0°, 15°, 30°, and 45°. The FEA results and nonlinear analytical analysis (numerical integration) results are then compared.

A. Nonlinearity of vertically loaded cantilever beam

First, the case where the cantilever beam was vertically loaded at the free end, i.e., $\gamma=0$, was treated. To get a general understanding of the effect of nonlinearity for cantilevered beams, the load and deflection expressions from linear and nonlinear analyses are normalized to yield nondimensional parameters as follows:

$$\frac{F_L L^2}{EI} = 2\phi_0, \qquad \frac{\delta_{yL}}{L} = \frac{2}{3}\phi_0, \tag{31}$$

and

$$\frac{F_N L^2}{EI} = [F(k) - F(\theta_1, k)]^2, \qquad \frac{\delta_{yN}}{L} = 1 - 2\frac{E(k) - E(\theta_1, k)}{F(k) - F(\theta_1, k)}, \tag{32}$$

where F_L and δ_{yL} are load and vertical deflection from linear analysis; F_N and δ_{yN} are load and vertical deflection from nonlinear analysis.

The relative error in force from linear analysis, $|(F_N - F_L)/F_N|$, provides a measure of the nonlinearity of the cantilever response. Figure 5(a) shows normalized load as a function of the slope at the free end obtained from each of the linear analysis, nonlinear analysis, and FEA. Figure 5(b) shows the corresponding force estimation error from linear analysis. The nonlinear effect becomes more significant with increasing cantilever deflection (and thus slope). At large deflection the linear analysis seriously underestimates the applied load. When the slope at the free end is ≈21° (a normalized vertical deflection of ≈0.25), there is an ≈5% error in the force from linear analysis. As shown in Table I, the angles of slope in our experiments were all less than 21°. Therefore, the linear analysis would not significantly underestimate the load if it were not for the fact that specimen misalignment was present in the experiments.

B. Nonlinearity of nonvertically loaded cantilever beam

The relatively large error in force from linear analysis shown in Table I is a combined result of large deflection and large loading angle (due to specimen misalignment), because either large deflection or large loading angle alone cannot induce such large error. As can be seen in Fig. 2, at large deflection (large δ_y) and large loading angle (large γ and thus large F_x), the bending moment term $M_x = F_x(\delta_y - y)$ plays an important role in the cantilever deflection. The contribution of this moment is neglected for linear response, which leads

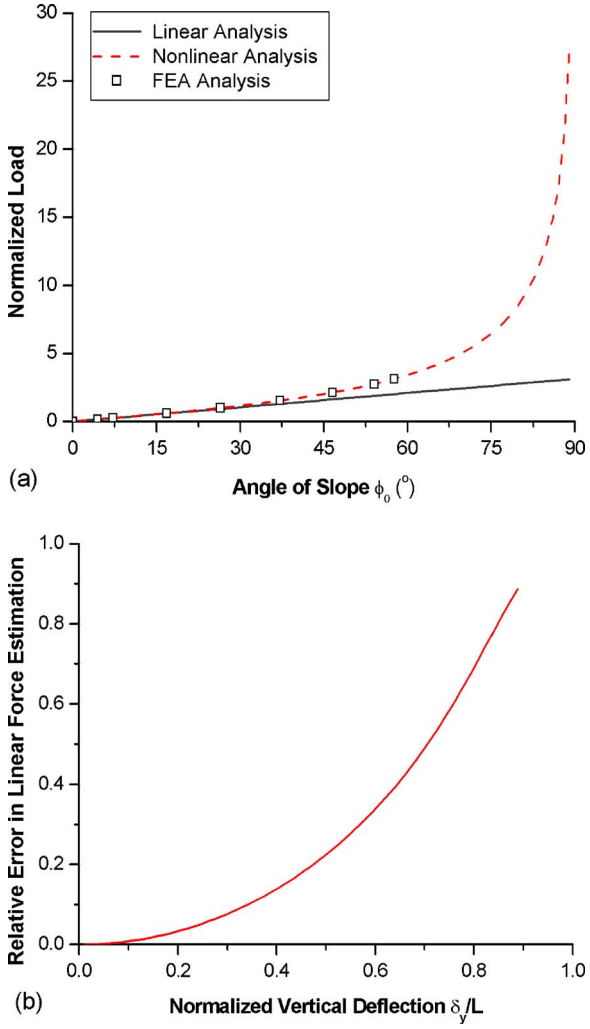

FIG. 5. (Color online) (a) Normalized load applied at the free end of a cantilever beam as a function of the slope at the free end from linear analysis, nonlinear analysis, and FEA. (b) Relative error in the applied load from the use of linear analysis as a function of the normalized vertical deflection.

to a large error in the force as shown in Table I. A detailed comparison of linear analysis, nonlinear analysis, and FEA results of a nonvertically loaded cantilever beam is provided next.

In linear analysis, the load (F_L) and the vertical deflection (δ_{yL}) at the free end of a nonvertically loaded cantilever beam are given by

$$F_L = K\delta_{yL}/\cos\gamma = 2\frac{EI\phi_0}{L^2\cos\gamma},$$
$$\delta_{yL} = \frac{2}{3}\phi_0 L. \tag{33}$$

In nonlinear analysis, the applied load (F_N) and vertical and horizontal deflections (δ_{yN}, δ_{xN}) at the free end are represented by Eqs. (21), (23), and (25), respectively.

Normalizing all the expressions to yield nondimensional parameters gives

$$\frac{F_L L^2}{EI} = 2\frac{\phi_0}{\cos\gamma},$$
$$\frac{\delta_{yL}}{L} = \frac{2}{3}\phi_0, \tag{34}$$

and

$$\frac{F_N L^2}{EI} = [F(k) - F(\theta_1,k)]^2,$$
$$\frac{\delta_{yN}}{L} = \left[1 - 2\frac{E(k) - E(\theta_1,k)}{F(k) - F(\theta_1,k)}\right]\cos\gamma - \frac{2k\cos\theta_1}{F(k) - F(\theta_1,k)}\sin\gamma, \tag{35}$$
$$\frac{\delta_{xN}}{L} = 1 - \left[1 - 2\frac{E(k) - E(\theta_1,k)}{F(k) - F(\theta_1,k)}\right]\sin\gamma - \frac{2k\cos\theta_1}{F(k) - F(\theta_1,k)}\cos\gamma.$$

Figure 6(a) shows the normalized load as a function of angle of loading with respect to different vertical deflections at the free end of the cantilever from analytical analysis and FEA. With an increase of loading angle, higher load is needed to achieve the same vertical deflection. As previously discussed, the angle of loading γ should be less than $\pi/2 - \phi_0$. As will be presented later in Fig. 8, for a given deflection there is a correlation between the slope and the loading angle; the larger the loading angle, the smaller the slope. The corresponding limits for the angle of loading (γ) for normalized deflections of 0.1, 0.25, and 0.5 are around 84°, 71°, and 58°. As shown in Fig. 6(a), when the loading angle approaches these limits, the normalized load rapidly increases.

Figure 6(b) shows the relative error in force from linear analysis, $|(F_A - F_L)/F_A|$, as a function of the angle of loading at different normalized vertical deflection values. As previously discussed, the beam nonlinearity is a combined result of large deflection and nonvertical loading. As can be seen in Fig. 6(b), at positive loading angle the nonlinear component of the response of the cantilever increases with increasing vertical deflection at the free end. At the same vertical deflection, the cantilever nonlinearity increases with increasing loading angle (while $\gamma > 0$).

When the loading angle is positive, the linear analysis always underestimates the applied load. As can be seen in Fig. 2, when the loading angle is negative, the bending moment induced by the F_x component contributes to the further deflection of the cantilever. The linear analysis (where the contribution of the F_x component is neglected) would then overestimate the load. As shown in Fig. 6(b), for each configuration there is a negative loading angle value at which the linear and analytical analysis yields the same load. When the loading angle becomes more negative, the linear analysis overestimates the applied load.

From Fig. 6 we can see that nonvertical loading induces a significant nonlinear effect. For example, a normalized vertical deflection of 0.25 achieved with vertical loading yields

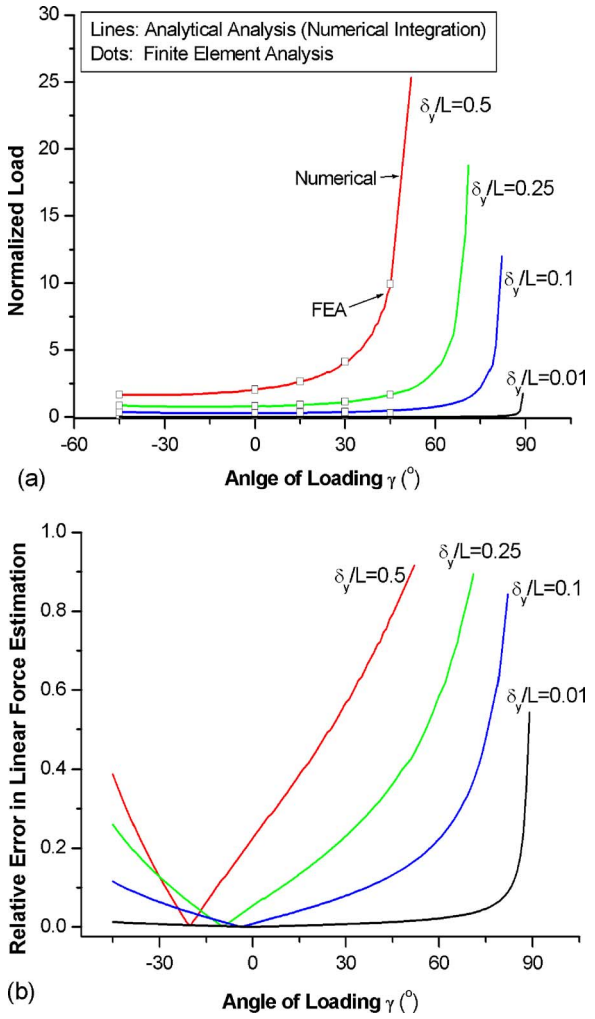

FIG. 6. (Color online) (a) Normalized applied load vs angle of loading at different normalized vertical deflections obtained from analytical analysis and FEA. (b) Relative error in the applied load from the use of linear analysis vs angle of loading at different normalized vertical deflections.

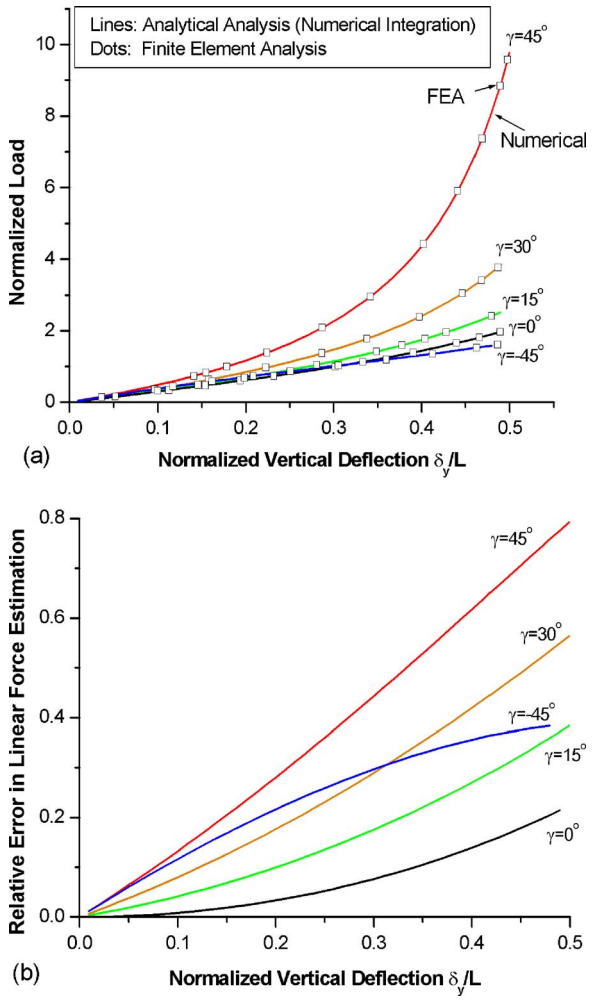

FIG. 7. (Color online) (a) Normalized applied load vs normalized vertical deflection at different angles of loading from analytical analysis and FEA. (b) Relative error in the applied load from the use of linear analysis vs normalized vertical deflection at different values of the loading angle.

an ≈5% error in force by the linear analysis, while same vertical deflection achieved with 30° loading angle has an error of ≈23%.

At small deflection the nonlinear effect is insignificant for a vertically loaded cantilever [Fig. 5(b)]. The nonlinear effect at small deflection for a nonvertically loaded cantilever is explored with the case of a normalized deflection of 0.01 (Fig. 6). As can be seen in Fig. 6(b), the nonlinear effect at small deflection for a nonvertically loaded beam is also insignificant until a very large angle of loading. For example, for a normalized deflection of 0.01, the relative error in force from linear analysis is only ≈5% at a large angle of loading of 76°.

Figure 7 presents the nonlinearity of a nonvertically loaded cantilever at large deflection from another perspective, namely, the relationship between the applied load and the vertical deflection at the free end of the cantilever. Figure 7(a) shows the relationship between the normalized load and normalized vertical deflection at the free end with respect to different angles of loading from nonlinear analytical analysis and FEA. Figure 7(b) shows the corresponding error in computed force from the linear analysis as a function of the normalized vertical deflection at the free end with respect to different angles of loading. Similar to Fig. 6, Fig. 7 clearly demonstrates an increase of cantilever nonlinearity with increasing cantilever deflection and/or increasing loading angle.

The relationship between the slope and vertical deflection at the free end under different loading conditions was also studied. At small deflection, there is a proportional relationship between the vertical deflection and the slope at the free end of a cantilever [shown in Eq. (1)]. Such a relationship will not hold at large deflection due to cantilever nonlinearity. Figure 8 shows the slope as a function of the normalized vertical deflection at the free end with respect to different loading angles from nonlinear analysis. The linear analysis relationship is also shown with a dashed line as a reference. When the normalized vertical deflection is less than 0.2, there is an essentially linear relationship between the slope and vertical deflection. At larger deflection, the curves from vertical and nonvertical loading all deviate from the linear case. Overall, the relationship between the slope and vertical deflection at the free end is not very sensitive to the angle of loading.

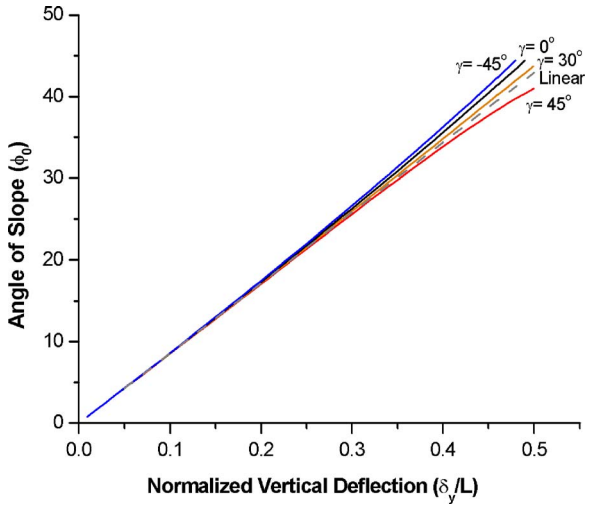

FIG. 8. (Color online) The slope vs normalized vertical deflection at the free end at different values of the loading angle.

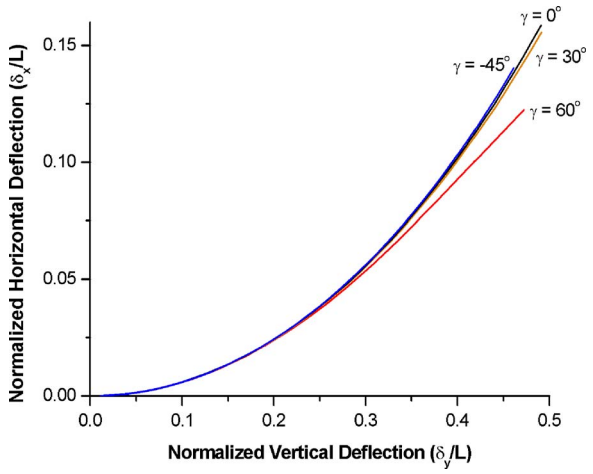

FIG. 9. (Color online) Normalized horizontal deflection vs normalized vertical deflection at the free end of a cantilever beam at different values of the loading angle.

Figure 9 shows the relationship between the normalized horizontal deflection and vertical deflection with respect to different angles of loading; this relationship is also not very sensitive to the loading angle. Figures 8 and 9 show that at the same vertical deflection, the slope and horizontal deflection is smaller at large loading angle, which means that the beam is less curved while being loaded at larger angle.

C. Comparison between FEA and analytical analysis

As demonstrated in Figs. 5–7, there is an excellent agreement between the nonlinear analytical analysis and FEA results. With commercial software such as MATLAB, the applied load at large deflection can be easily calculated from the analytical expression through numerical integration, while it is relatively time consuming to build a FEA model. While not straightforward, the analytical expressions present the relationships among the parameters such as load, deflection, slope, and loading angle. Such kinds of relationships cannot be easily seen in FEA. In addition, the analytical analysis is more suitable for experimental data analysis to obtain the load. When the deflection of a microcantilever is used as the force-sensing mode, the slope and angle of loading are the known parameters while the load is unknown. On the other hand, FEA is more suitable to determine the beam response at a given load.

D. Applications

The detailed comparison presented above is useful in experimental design and data analysis, where cantilever beams are used as the force-sensing or actuating elements and the nonlinear response is needed. Figure 5 can be readily used as a quick reference to determine the error in sensed or applied load from an assumed linear response for vertically loaded cantilever beams. For example, if the slope at the free end is less than 21° (or the vertical deflection at the free end is less than 1/4 of the beam length), the load calculated with Hooke's law could be used to approximate the true applied load (with $<5\%$ error).

If the concentrated load is not applied vertically, Figs. 6 and 7 can serve as references to quickly estimate the force error from linear analysis. Based on an estimate of the loading angle and either the vertical deflection or the slope at the free end, one can easily tell the error from linear analysis for each loading situation, from Figs. 6(b) and 7(b). For example, if a cantilever loaded at 30° angle is deflected to 1/4 of its length, one should expect a 23% error if the applied load is obtained by linear analysis, with the actual load being about 1.3 times that obtained from an assumed linear response.

VI. CONCLUSIONS

AFM cantilevers were used as force-sensing elements in our nanoscale tensile testing experiments on TCNTs inside a SEM. Large deflection of the cantilever beam occurred in the tests along with nonideal specimen alignment. Analytical expressions were obtained for the applied load and cantilever deflections. Numerical integration was used to obtain the breaking forces of the TCNTs, based on the measured slope and loading angle obtained from recorded SEM images. The influence of the loading position was discussed, and an effective beam length approximation was proposed for the cases where the loads were applied at an AFM tip. A comparison was made between the applied load obtained from linear and nonlinear analyses. Due to nonlinear effects, the linear analysis underestimates the true load by up to 15%.

The cantilever nonlinearity induced by large deflection and nonvertical loading with the analytical analysis and FEA was then further assessed. Excellent agreement was obtained between the results from analytical analysis and FEA. The cantilever nonlinearity was found to increase with increasing cantilever deflection and/or angle of loading. The slope and cantilever deflections were found to be not very sensitive to the angle of loading. The results presented in this paper can be used to quickly estimate the true loads in a variety of situations where cantilever beams are used as force-sensing or actuating elements.

ACKNOWLEDGMENTS

This work is supported by the National Science Foundation (NIRT Program, Grant No. 0304506, Dr. Ken P. Chong, Program Director) and by NASA (Award No. NCC-1-02037) through the University Research, Engineering, and Technology Institute on Bio-inspired Materials (BiMat). The SEM work was performed in the EPIC facility of the NUANCE Center at Northwestern University. The NUANCE Center is supported by NSF-NSEC, NSF-MRSEC, Keck Foundation, the State of Illinois, and Northwestern University.

[1] J. P. Salvetat, J. M. Bonard, N. H. Thomson, A. J. Kulik, L. Forro, W. Benoit, and L. Zuppiroli, Appl. Phys. A: Mater. Sci. Process. **69**, 255 (1999).
[2] A. H. Barber, S. R. Cohen, and H. D. Wagner, Appl. Phys. Lett. **82**, 4140 (2003).
[3] M. F. Yu, M. J. Dyer, G. D. Skidmore, H. W. Rohrs, X. K. Lu, K. D. Ausman, J. R. Von Ehr, and R. S. Ruoff, Nanotechnology **10**, 244 (1999).
[4] M. F. Yu, B. S. Files, S. Arepalli, and R. S. Ruoff, Phys. Rev. Lett. **84**, 5552 (2000).
[5] M. F. Yu, O. Lourie, M. J. Dyer, K. Moloni, T. F. Kelly, and R. S. Ruoff, Science **287**, 637 (2000).
[6] X. Chen, S. Zhang, D. A. Dikin, W. Ding, R. S. Ruoff, L. Pan, and Y. Nakayama, Nano Lett. **3**, 1299 (2003).
[7] E. Zussman, X. Chen, W. Ding, L. Calabri, D. A. Dikin, J. P. Quintana, and R. S. Ruoff, Carbon **43**, 2175 (2005).
[8] W. Ding, L. Calabri, X. Chen, K. M. Kohlhaas, and R. S. Ruoff, Compos. Sci. Technol. **66**, 1109 (2006).
[9] W. Ding, L. Calabri, K. M. Kohlhaas, D. A. Dikin, and R. S. Ruoff, Exp. Mech. s11340-006-9344-6 (in press).
[10] W. Rong, W. Ding, L. Madler, R. S. Ruoff, and S. K. Friedlander, Nano Lett. **6**(12), 2646 (2006).
[11] T. T. Xu, R. D. Piner, and R. S. Ruoff, Langmuir **19**, 1443 (2003).
[12] T. T. Xu, F. T. Fisher, L. C. Brinson, and R. S. Ruoff, Nano Lett. **3**, 1135 (2003).
[13] W. Ding, D. A. Dikin, X. Chen, X. Wang, X. Li, R. Piner, R. S. Ruoff, and E. Zussman, J. Appl. Phys. **98**, 014905 (2005).
[14] K. Bisshopp and D. Drucker, Q. Appl. Math. **3**, 272 (1945).
[15] K. Bisshopp, Q. Appl. Math. **30**, 521 (1973).
[16] T. Belendez, C. Neipp, and A. Belendez, Eur. J. Phys. **23**, 371 (2002).
[17] The elliptical integral subroutines used in the numerical integration program were downloaded from http://ceta.mit.edu/comp_spec_func/. The copyright belongs to the Center for Electromagnetic Theory and Applications, Research Lab of Electronics and Department of Electrical Engineering and Computer Science, Massachusetts Institute of Technology.
[18] J. J. Wortman and R. A. Evans, J. Appl. Phys. **36**, 153 (1965).
[19] C. Y. Li, R. S. Ruoff, and T. W. Chou, Compos. Sci. Technol. **65**, 2407 (2005).
[20] E. P. S. Tan, C. N. Goh, C. H. Sow, and C. T. Lim, Appl. Phys. Lett. **86**, 073115 (2005).
[21] E. W. Wong, P. E. Sheehan, and C. M. Lieber, Science **277**, 1971 (1997).
[22] J. H. Song, X. D. Wang, E. Riedo, and Z. L. Wang, Nano Lett. **5**, 1954 (2005).